Defence Research and Development Canada
Recherche et développement pour la défense Canada

DEFENCE R&D DÉFENSE

Moving Target Parameter Estimation for RADARSAT-2 MODEX

S. Chiu

Defence R&D Canada – Ottawa
TECHNICAL MEMORANDUM
DRDC Ottawa TM 2005-214
December 2005

Canada

Moving Target Parameter Estimation for RADARSAT-2 MODEX

S. Chiu
Defence R&D Canada – Ottawa

Defence R&D Canada – Ottawa

Technical Memorandum

DRDC Ottawa TM 2005-214

December 2005

Author

S. Chiu

Approved by

Doreen Dyck
Head/Radar Systems Section

Approved for release by

Anthony Ashley
Chair/Document Review Panel

Abstract

Moving target parameter estimation algorithms have been developed previously for airborne (or flat Earth) geometry. Subtle differences exist in migrating from a flat stationary Earth geometry to a spherical rotating Earth geometry. Factors, such as orbital parameters and spacecraft centripetal acceleration, must be taken into account. In addition, the dynamic antenna squint implemented in the RADARSAT-2 satellite for Earth motion compensation needs to be modelled into the algorithms. This technical memorandum derives the spaceborne version of the algorithm, based on the fractional Fourier transform and along-track interferometry, previously developed for the Convair 580 radar.

Résumé

Des algorithmes d'estimation des paramètres des cibles mobiles ont été établis précé-demment pour une géométrie aérienne (Terre plate). De subtiles différences se manifestent au moment où l'on abandonne la géométrie à Terre stationnaire et plate pour adopter la géométrie à Terre tournante et sphérique. Des facteurs comme les paramètres orbitaux et l'accélération centripète de l'engin spatial doivent être pris en compte. Par ailleurs, le strabisme dynamique de l'antenne, incorporé au satellite RADARSAT-2 pour compenser le mouvement de la Terre, doit être modélisé dans l'algorithme. Le présent mémoire technique établit la version spatiale de l'algorithme fondé sur une transformée de Fourier fractionnaire et sur l'interférométrie longitudinale, précédemment mis au point pour le radar Convair 580.

This page intentionally left blank.

Executive summary

Background

Canada's RADARSAT-2 commercial SAR satellite, to be launched in Spring 2006, will have an experimental mode, called MODEX for Moving Object Detection EXperiment, that will allow the full antenna to be configured as two sub-apertures with two parallel receivers to define two independent data channels [1]. These two sub-apertures, arranged to lie along the flight path, record two echoes (the dual-receive mode), one from each section for every pulse transmitted at the full antenna. The two apertures enable one to detect targets with non-zero across-track velocity by providing essentially two identical views of the observed scene but at slightly different times. One of the major deficiencies in a two-aperture synthetic aperture radar (SAR) system is its inability to simultaneously cancel the clutter and to estimate target parameters. Along-track interferometry is often the technique used to estimate the target's across-track velocity, but the interferogram is always contaminated by unwanted stationary clutter.

Principal results

The fractional Fourier transform (FrFT) is a versatile, yet relatively unknown, signal processing tool that can be used to both maximize the signal-to-clutter ratio and allow target parameters to be estimated in the fractional Fourier domain using a few derived equations in closed form. The target parameter algorithm based on fractional Fourier transform has been developed previously for airborne (flat, stationary Earth) geometry and tested against Convair 580 data. Subtle differences exist in migrating from a flat stationary Earth geometry to a spherical rotating Earth geometry. Factors, such as orbital parameters and spacecraft centripetal acceleration, must be taken into account. In addition, the dynamic antenna squint implemented in RADARSAT-2 satellite for Earth motion compensation needs to be modelled into the algorithm.

The signal model describing a target moving in a spherical rotating Earth is first developed. This signal model is rigorous but its usefulness is limited, however, in that it cannot be expressed easily in a form that can be readily used to construct the target's range history and the SAR reference function. A simplified two-dimensional signal model is developed and the spherical three-dimensional model is used to verify equivalence. Using the simplified model, the target parameter estimation algorithm is derived for RADARSAT-2's MODEX and tested against simulated data.

Significance of results

This work is the first to address moving target parameter estimation in the RADARSAT-2 MODEX context. The developed signal model and the estimation algorithm take into account RADARSAT-2's dynamic antenna squint, Earth motion, and the radar's centripetal acceleration. The inclusion of these effects allows the accurate estimation of target velocity and position.

Future Work

Accurate ground moving target indication (GMTI) and target parameter estimation can be achieved only after sufficient suppression of interfering stationary clutter, particularly for space-based SARs with typically small exo-clutter regions. In its simplest form, GMTI is accomplished using two radar receiver channels, such as the dual receive antenna mode of RADARSAT-2's MODEX. It is well known, however, that a two-aperture approach to GMTI is sub-optimal and that target parameter estimation is often compromised by clutter interference or poor signal-to-clutter ratios. Two degrees of freedom are simply not enough to simultaneously suppress the clutter and to accurately estimate the target's properties, such as velocity and location.

In order to take advantage of efficient space-time adaptive processing (STAP) techniques, multi-channel SAR systems with more than two channels are required. Several concepts for increasing the spatial diversity for RADARSAT-2, that will allow the two-channel SAR system to operate like a three or four channel radar, should be explored. Owing to the very flexible programming capabilities of the RADARSAT-2 antenna, this can either be accomplished by transmitter toggling between subsequent pulses or via intelligent transmitter/receiver excitation schemes. A trade-off analysis between number of channels, phase center separation, and PRF limitation should be carried out based on RADARSAT-2 MODEX parameters.

Although the developed parameter estimation algorithm is applied to a two-aperture SAR data, the technique can be easily extended to three- or four-aperture systems.

S. Chiu; 2005; Moving Target Parameter Estimation for RADARSAT-2 MODEX; DRDC Ottawa TM 2005-214; Defence R&D Canada - Ottawa.

Sommaire

Contexte

Le satellite SAR commercial RADARSAT-2 du Canada, qui doit être lancé au printemps 2006, comportera un mode expérimental (appelé MODEX pour faire référence à l'expérience de détection des objets mobiles), qui permettra de diviser l'antenne complète en deux sous-ouvertures dotées de deux récepteurs parallèles pour définir deux canaux de données indépendants [1]. Ces deux sous-ouvertures, disposées le long de la trajectoire de vol, enregistrent deux échos (mode de réception double), un en provenance de chaque aile, pour chacune des impulsions transmises à l'antenne complète. Les deux ouvertures peuvent détecter les cibles à vitesse transversale non nulle en procurant essentiellement deux vues identiques de la scène observée, mais à des instants légèrement différents. L'une des principales lacunes du radar à ouverture synthétique (SAR) à deux ouvertures tient à son incapacité à effectuer simultanément une annulation du clutter et une estimation des paramètres des cibles. On recourt souvent à l'interférométrie longitudinale pour estimer la vitesse transversale des cibles, mais l'interférogramme est toujours contaminé par le clutter fixe non désiré.

Principaux résultats

La transformée de Fourier fractionnaire constitue un outil de traitement des signaux polyvalent, bien que relativement peu connu, qui peut servir à maximiser le rapport signal/clutter et à estimer les paramètres des cibles dans le domaine de Fourier fractionnaire au moyen de quelques équations dérivées en forme fermée. Un algorithme des paramètres de cible fondé sur une transformée de Fourier fractionnaire a été élaboré précédemment pour une géométrie aérienne (Terre stationnaire et plate) et vérifié à l'aide des données du Convair 580. De subtiles différences se manifestent au moment où l'on abandonne la géométrie à Terre stationnaire et plate pour adopter la géométrie à Terre tournante et sphérique. Des facteurs comme les paramètres orbitaux et l'accélération centripète de l'engin spatial doivent être pris en compte. Par ailleurs, le strabisme dynamique de l'antenne, incorporé au satellite RADARSAT-2 pour compenser le mouvement de la Terre, doit être modélisé dans l'algorithme. On a élaboré un modèle de signal décrivant une cible mobile pour une Terre tournante et sphérique. Bien que rigoureux, ce modèle n'offre toutefois qu'une utilité limitée, car il est impossible de l'exprimer aisément sous une forme non vectorielle bien adaptée à la constitution de l'historique de distance des cibles et à la fonction de référence du SAR. Un modèle de signal bidimensionnel simplifié a été élaboré, et le modèle tridimensionnel sphérique a permis d'en vérifier l'équivalence. À l'aide du modèle simplifié, l'algorithme d'estimation des paramètres des cibles a été établi pour le MODEX de RADARSAT-2 et mis à l'essai au moyen de données de simulation.

Portée

Ces recherches sont les premières à porter sur l'estimation des paramètres des cibles mobiles dans le contexte du MODEX de RADARSAT-2. Le modèle de signal élaboré et l'algorithme d'estimation tiennent compte du strabisme dynamique de l'antenne de RADARSAT-2, des mouvements de la Terre et de l'accélération centripète du radar. L'inclusion de ces effets permet une estimation précise de la vitesse et de la position des cibles.

Recherches futures

L'efficience en matière d'indication des cibles terrestres mobiles (GMTI) et d'estimation des paramètres des cibles ne sera possible qu'après une suppression suffisante du clutter fixe brouilleur, surtout dans le cas des SAR spatiaux typiquement caractérisés par de petites régions d'exo-clutter. Sous sa forme la plus simple, cette suppression s'effectue au moyen de deux canaux de récepteur radar, comme dans le mode à deux antennes de réception du MODEX de RADARSAT-2. On n'ignore toutefois pas que la technique des deux ouvertures pour la GMTI n'est pas optimale et que du clutter brouilleur ou de mauvais rapports signal/bruit compromettent souvent l'estimation des paramètres des cibles. Deux degrés de liberté ne suffisent simplement pas à effectuer simultanément la suppression du clutter et l'évaluation précise des propriétés des cibles, comme la vitesse et la position.

Afin de tirer parti de techniques efficaces de traitement adaptatif espace-temps (STAP), il est nécessaire de recourir à des systèmes SAR comportant plus de deux canaux. On devrait examiner plusieurs techniques susceptibles d'accroître la diversité spatiale de RADARSAT-2 afin de faire fonctionner le système SAR à deux canaux presque comme un radar à trois ou à quatre canaux. Grce à la très grande souplesse de programmation de l'antenne RADARSAT-2, ce résultat peut s'obtenir soit par le basculement de l'émetteur entre des impulsions subséquentes, soit par des systèmes intelligents d'excitation d'émetteur et de récepteur. Il serait bon de mener une analyse de compromis entre le nombre de canaux, l'espacement des centres de phase et la limitation de la fréquence de répétition des impulsions, en se fondant sur les paramètres du MODEX de RADARSAT-2. Bien que l'algorithme élaboré pour l'estimation des paramètres se soit appliqué aux données d'un SAR à deux ouvertures, cette technique peut et doit tre étendue aux systèmes à trois ou à quatre ouvertures.

S. Chiu; 2005; Moving Target Parameter Estimation for RADARSAT-2 MODEX; DRDC Ottawa TM 2005-214; R & D pour la défense Canada - Ottawa.

Table of contents

List of figures

1 Introduction

Canada's RADARSAT-2 commercial SAR satellite, to be launched in Spring 2006, will have an experimental mode (called MODEX for Moving Object Detection EXperiment) that will allow the full antenna to be configured as two sub-apertures with two parallel receivers to define two independent data channels [1]. These two sub-apertures, arranged to lie along the flight path, record two echoes (the dual-receive mode), one from each wing for every pulse transmitted at the full antenna. The two apertures enable one to detect targets with non-zero across-track velocity by providing, essentially, two identical views of the observed scene but at slightly different times. Recently, several new detection techniques for two-channel SAR ground moving target indication (GMTI), including their statistical performance, have been proposed, e.g. [2]. It can be shown that a moving target with an across-track velocity v_{tr} causes a differential phase shift $4\pi v_{tr}\tau/\lambda$ (τ is the time between two observations and λ is wavelength), which may be detected by interferometric combination of the signals from a two-channel along-track SAR system [8]. For two-channel ATI, the measured differential phase will be contaminated by the overlapping stationary clutter, leading to errors in velocity and position estimates. In order to accurately estimate a target's true position and velocity, clutter contamination of the signal must be minimized. A relatively new signal processing tool, called the fractional Fourier Transform (FrFT), is used in combination with along-track interferometry (ATI) to maximize the signal-to-clutter ratio and to estimate moving target parameters. This technical memorandum describes the spaceborne version of an algorithm previously developed by Chiu [14] for the Convair 580 radar.

2 Signal Model in Spaceborne Geometry

In order to carry out target parameter estimation, an accurate target signal model must first be established. Unlike an airborne radar, the spacecraft cannot be assumed to be moving above a flat stationary earth. Orbital parameters and spacecraft centripetal acceleration must be taken into account. The spherical geometry orbital model is probably the most accurate one, but its modelling complexity makes the resulting range history equation too complex for use in the derivation of target motion and position parameters. A simplified two-dimensional model is convenient and useful for theoretical analyses and derivations but its accuracy must be first established by comparing its generated range history with that of the full orbital model before it can be applied in the subsequent algorithm development. In the following two sub-sections, the two models are developed, analyzed, compared, and the equivalence of the two models established. The Taylor expansion approximation of the signal model is also examined to ensure its validity in the subsequent theoretical

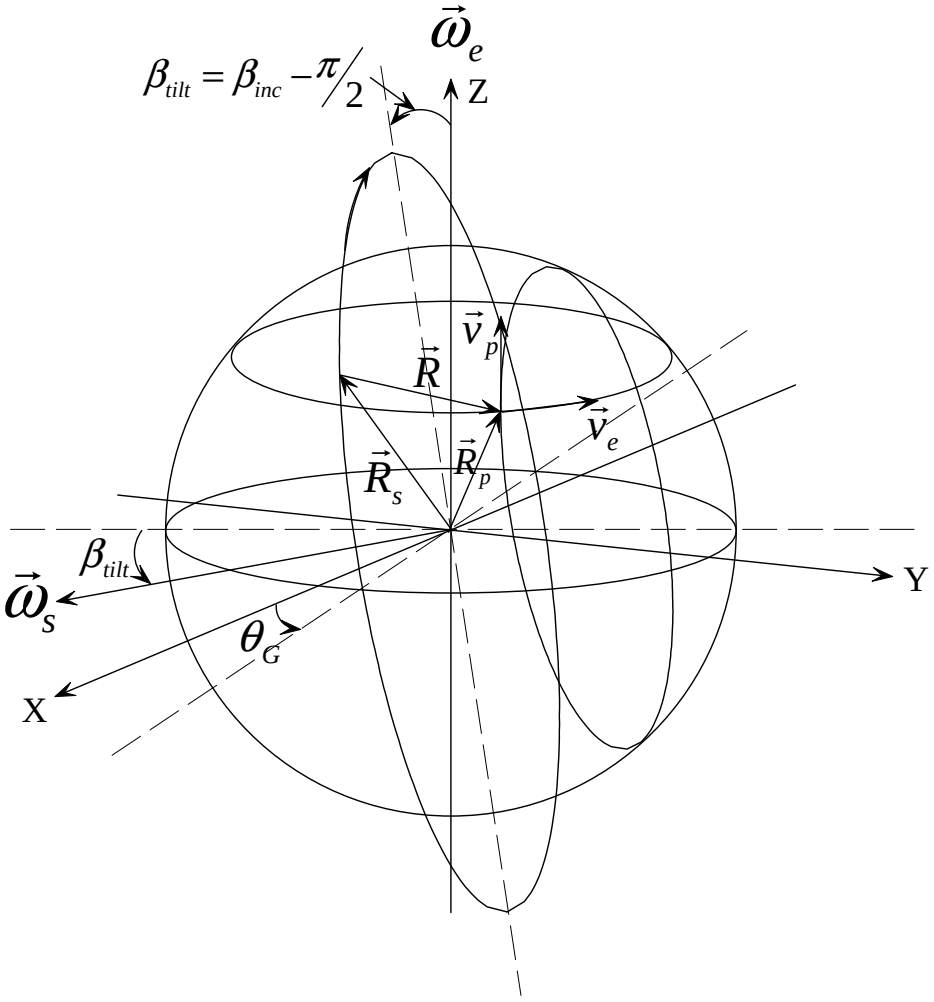

Figure 1: *RADARSAT-2 orbital geometry and parameters*

derivations of target parameters, which make use of the parabolic approximation. The radial acceleration component introduced by the spacecraft's circular orbital motion is examined and its impact on parameter estimation discussed.

2.1 Orbital model

A spherical geometry orbital signal model is most easily developed in vector format. The orbital geometry is depicted in Fig. 1. We construct a spacecraft orbital

propagation vector which begins on the x-axis as

$$\vec{R}_s = R_s \begin{bmatrix} 1 \\ 0 \\ 0 \end{bmatrix}, \tag{1}$$

where R_s is the spacecraft orbital radius, which is 7,170 km for RADARSAT-2. We then let $\vec{R}_s$ rotate about the y-axis at an angular velocity ω_s rad/s, which is calculated from

$$\omega_s = \sqrt{\frac{GM_e}{R_s^3}}, \tag{2}$$

where G is gravitational constant and M_e is the mass of the Earth. The resulting $\vec{R}_s$ becomes

$$\vec{R}_s = \mathbf{M}_y(\theta_0 + \omega_s t) R_s \begin{bmatrix} 1 \\ 0 \\ 0 \end{bmatrix}, \tag{3}$$

where $\mathbf{M}_y(\omega_s t)$ rotates $\vec{R}_s$ around the y-axis at an angular speed ω_s:

$$\mathbf{M}_y(\theta_0 + \omega_s t) = \begin{bmatrix} \cos(\theta_0 + \omega_s t) & 0 & -\sin(\theta_0 + \omega_s t) \\ 0 & 1 & 0 \\ \sin(\theta_0 + \omega_s t) & 0 & \cos(\theta_0 + \omega_s t) \end{bmatrix}. \tag{4}$$

The angle θ_0 is related to the latitude (θ_{lat}) of the radar beam center on the ground at time zero. To account for an orbital inclination, β_{inc}, we multiply (3) by the rotation matrix $\mathbf{M}_x(\beta_{tilt})$ about the x-axis, which rotates the satellite orbital plane an angle β_{tilt} away from z-axis, where $\beta_{tilt} = \beta_{inc} - 90^\circ$. This results in

$$\vec{R}_s = \mathbf{M}_x(\beta_{tilt}) \mathbf{M}_y(\theta_0 + \omega_s t) R_s \begin{bmatrix} 1 \\ 0 \\ 0 \end{bmatrix}, \tag{5}$$

where

$$\mathbf{M}_x(\beta_{tilt}) = \begin{bmatrix} 1 & 0 & 0 \\ 0 & \cos\beta_{tilt} & -\sin\beta_{tilt} \\ 0 & \sin\beta_{tilt} & \cos\beta_{tilt} \end{bmatrix}. \tag{6}$$

If the spacecraft's position vector at the Equator forms an angle θ_G with respect to x-axis, then the resulting satellite orbital propagation vector is given by

$$\boxed{\vec{R}_s = \mathbf{M}_z(\theta_G) \mathbf{M}_x(\beta_{tilt}) \mathbf{M}_y(\theta_0 + \omega_s t) R_s \begin{bmatrix} 1 \\ 0 \\ 0 \end{bmatrix}}, \tag{7}$$

where

$$\mathbf{M}_z(\theta_G) = \begin{bmatrix} \cos\theta_G & -\sin\theta_G & 0 \\ \sin\theta_G & \cos\theta_G & 0 \\ 0 & 0 & 1 \end{bmatrix}. \tag{8}$$

The vector describing the motion of the radar beam center on the ground can be similarly constructed and shown to be

$$\boxed{\vec{R}_p(t) = \mathbf{M}_z(\theta_G)\mathbf{M}_x(\beta_{tilt})[\mathbf{M}_y(\theta_0 + \omega_s t)R_e \cos\chi \begin{bmatrix} 1 \\ 0 \\ 0 \end{bmatrix} + \vec{L}]}, \tag{9}$$

where χ is the angle between the beam center vector $\vec{R}_p$ and the spacecraft propagation vector $\vec{R}_s$ as depicted in Fig. 1 and R_e is the Earth radius. $\mathbf{L}$ is a translation vector given by

$$\vec{L} = \begin{bmatrix} 0 \\ R_e \sin\chi \\ 0 \end{bmatrix}. \tag{10}$$

From Fig. 6(a), it can be seen that $\chi = \theta_i - \phi$, where θ_i is the angle of incidence and ϕ is the angle of depression.

The latitude of the beam center is given by

$$\theta_{lat} = \frac{\pi}{2} - \text{acos}\left[\frac{\vec{\omega}_e \bullet \vec{R}_p}{|\vec{\omega}_e||\vec{R}_p|}\right], \tag{11}$$

and the longitude is computed from

$$\theta_{long} = \text{acos}\left[\frac{\vec{R}_{pxy} \bullet \hat{X}}{|\vec{R}_{pxy}|}\right], \tag{12}$$

where $\vec{R}_{pxy}$ is the $\vec{R}_p$ vector projected onto XY plane (i.e. setting the z-component of $\vec{R}_p$ to zero), $\hat{X}$ is the unit vector in the direction of X-axis, and $\vec{\omega}_e$ is the Earth rotation vector as depicted in Fig. 1.

The Earth angular velocity vector is given by

$$\vec{\omega}_e = \omega_e \begin{bmatrix} 0 \\ 0 \\ 1 \end{bmatrix}, \tag{13}$$

where ω_e is the Earth angular velocity in rad/s. The satellite angular velocity vector can be shown to be

$$\vec{\omega}_s = \mathbf{M}_z(\theta_G)\mathbf{M}_x(\beta_{tilt})\omega_s \begin{bmatrix} 0 \\ -1 \\ 0 \end{bmatrix}. \tag{14}$$

Using the above equations, the Earth surface velocity vector $\vec{v}_e$ at the beam center $\vec{R}_p$ is given by

$$\vec{v}_e(t) = \vec{\omega}_e \times \vec{R}_p(t), \tag{15}$$

the beam ground velocity vector $\vec{v}_p$ given by

$$\vec{v}_p = \vec{\omega}_s \times \vec{R}_p(t), \tag{16}$$

and the satellite velocity vector $\vec{v}_s$ by

$$\vec{v}_s = \vec{\omega}_s \times \vec{R}_s(t). \tag{17}$$

The unit vector in the along-track and across-track directions (on the ground and in the slant range) can be written as

$$\begin{aligned} \hat{x} &= \frac{\vec{v}_{p0}}{|\vec{v}_{p0}|}, \\ \hat{y} &= \frac{\vec{v}_{p0} \times \vec{R}_{p0}}{|\vec{v}_{p0} \times \vec{R}_{p0}|}, \\ \hat{r} &= \frac{\vec{R}_{p0} - \vec{R}_{s0}}{|\vec{R}_{p0} - \vec{R}_{s0}|}, \end{aligned} \tag{18}$$

respectively. The additional subscript '0' indicates $t = 0$. The components of the Earth surface velocity in along-track and across-track directions (on the ground and in slant range) are then given by

$$\begin{aligned} v_{ex0} &= \vec{v}_{e0} \bullet \hat{x}, \\ v_{ey0} &= \vec{v}_{e0} \bullet \hat{y}, \\ v_{er0} &= \vec{v}_{e0} \bullet \hat{r}, \end{aligned} \tag{19}$$

respectively. The RADARSAT-2 applies a dynamic antenna beam squint to compensate for Earth rotation [6]. This antenna beam squint angle ϕ_s can be modelled as

$$x_0 = r_0 \tan \phi_s + \delta x_0, \tag{20}$$

where x_0 is the target azimuth position, $r_0 \tan \phi_s$ is the squinted antenna beam center azimuth position on the ground, and δx_0 the target azimuth distance from the beam center at time zero. In order to compensate for Earth rotation, the squint angle is set to

$$\boxed{\phi_s = \text{atan}\left(\frac{v_{er}}{v_s - v_{ex}}\right)}, \tag{21}$$

where $v_s = |\vec{v}_s|$ is the platform velocity. The derivation of this formula will be given in Sec. 2.2.

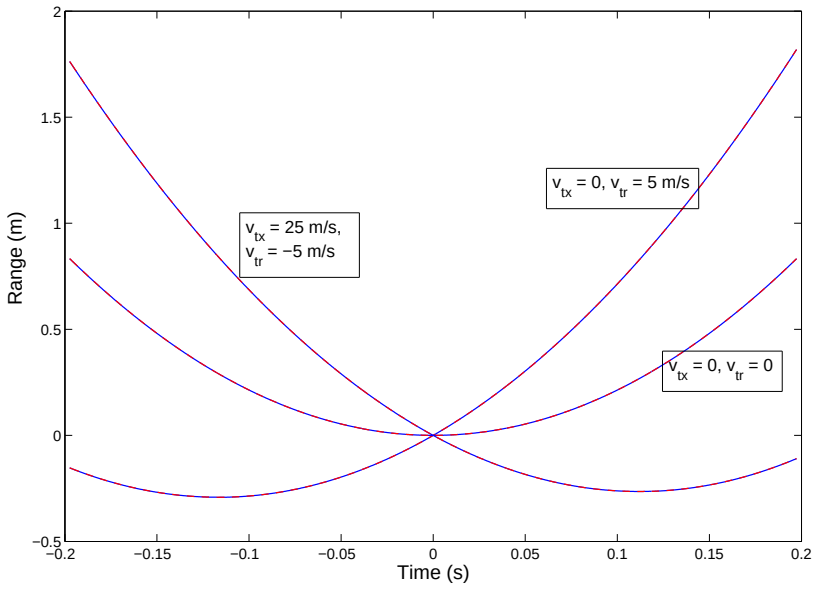

Figure 2: *Range histories of a target moving at three different velocities: (a)* $v_{tx} = 0$, $v_{tr} = 0$, *(b)* $v_{tx} = 0$, $v_{tr} = 5$ *m/s, and (c)* $v_{tx} = 25$ *m/s,* $v_{tr} = -5$ *m/s. The blue lines are generated using spherical 3-D orbital model (Sec. 2.1) and the red lines are generated using a simplified 2-D model (Sec. 2.2).*

We construct the target motion vector $\vec{R}_t$ to give

$$\vec{R}_t = \vec{R}_{p0} + [x_0 + (v_{tx} + v_{ex0})t]\hat{x} + (v_{tr} + v_{er0})t\hat{r}, \tag{22}$$

where v_{tx} and v_{tr} are target azimuth and slant range velocities, respectively. Then the range history $R(t)$ of the target with respect to the radar is

$$R(t) = |\vec{R}_t - \vec{R}_s| - R_0, \tag{23}$$

where $R_0 = |\vec{R}_{t0} - \vec{R}_{s0}|$. The range histories of a moving target, generated using the above model, are shown in blue in Fig. 2 for three different target velocities.

Another question that needs to be addressed is whether the dynamic-antenna-squint corrected Earth motion does in fact yield the same range history as that without dynamic squint correction but for a stationary Earth. This can be answered by setting the Earth motion to zero and removing the antenna squint in our model to yield range histories of the same target moving in a stationary Earth for comparison purposes. The results of this comparison are shown in Fig. 3 and are obtained for targets moving only in the range direction (i.e., targets have zero along-track

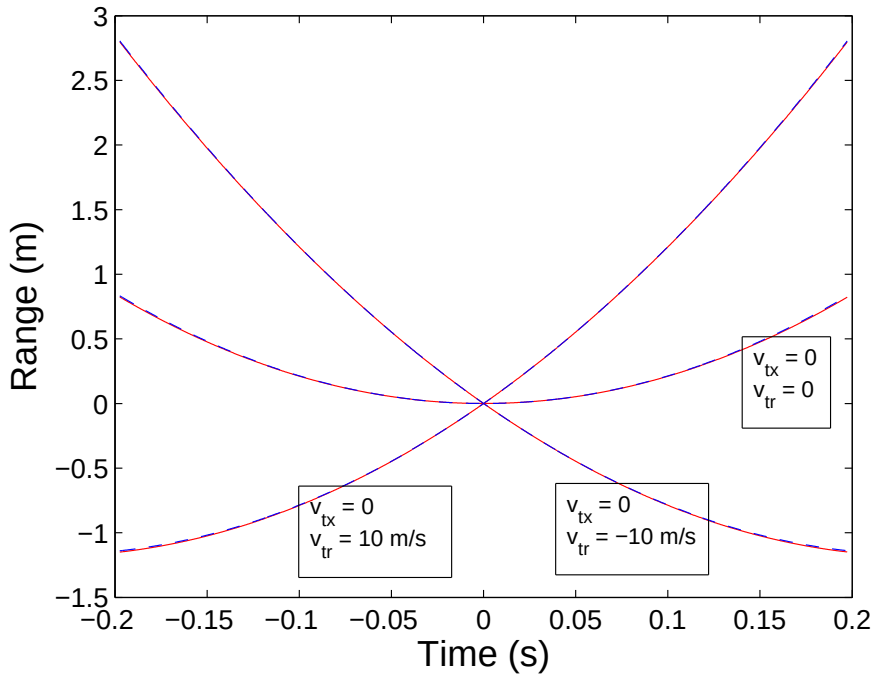

Figure 3: *Range histories of a target moving at three different velocities: (a)* $v_{tx} = 0$, $v_{tr} = 0$, *(b)* $v_{tx} = 0$, $v_{tr} = 10$ *m/s, and (c)* $v_{tx} = 0$, $v_{tr} = -10$ *m/s. The red lines are generated using the stationary Earth model and the blue lines are generated using the rotating Earth model with a dynamic antenna squint compensation computed using (21). The 2-D model is used.*

velocity). The dynamic antenna squint appears to compensate well for Earth motion. However, when the targets also have along-track motion, the results no longer agree if one uses (21) to compute the squint angle ϕ_s. The discrepancy can be seen in Fig. 4, which shows the range histories of targets with $v_{tx} \neq 0$ for cases with (rotating Earth) and without (stationary Earth) the dynamic squint compensation. If we, however, modify (21) to include the target along-track velocity as (to be derived in Sec. 2.2)

$$\boxed{\phi_s = \text{atan}\left(\frac{v_{er}}{v_s - v_{ex} - v_{tx}}\right)}, \tag{24}$$

then the resulting Earth-motion compensated range history of the target with $v_{tx} \neq 0$ can be shown to agree well with that of the same target moving in the stationary Earth as seen Fig. 5. Therefore, full Earth motion compensation using an antenna squint requires the knowledge of the moving target's along-track (azimuth) velocity. But this is a parameter that needs to be estimated and is not known *a priori*. Even if it is known, the compensation for multiple targets of varying azimuth velocities can-

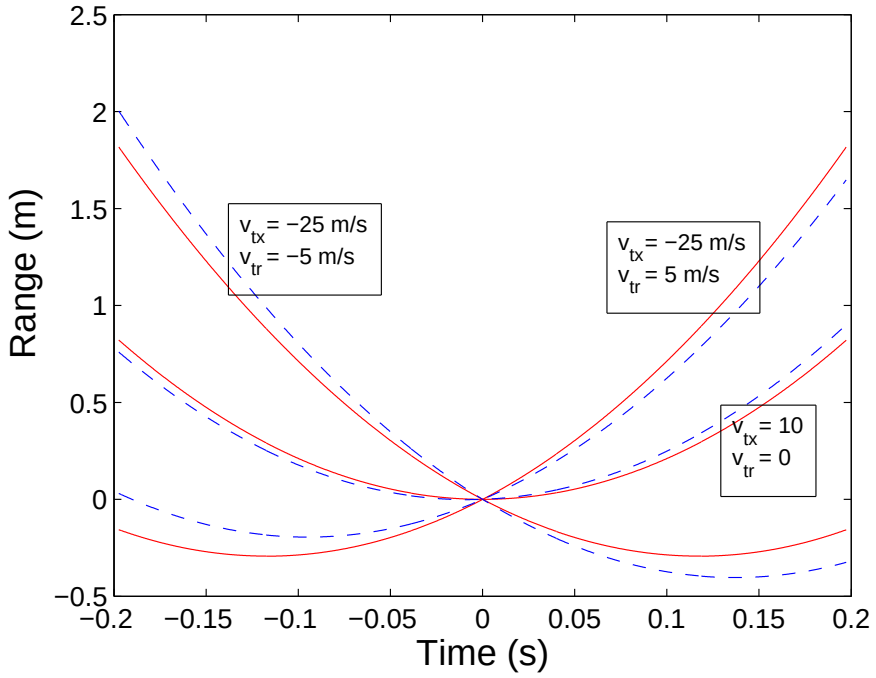

Figure 4: *Range histories of a target moving at three different velocities: (a) $v_{tx} = 0$, $v_{tr} = 10$ m/s, (b) $v_{tx} = -25$, $v_{tr} = 5$ m/s, and (c) $v_{tx} = -25$ m/s, $v_{tr} = -5$ m/s. The red lines are generated using the stationary Earth model and the blue lines are generated using the moving Earth model with a dynamic antenna squint compensation computed using (21). The 2-D model is used.*

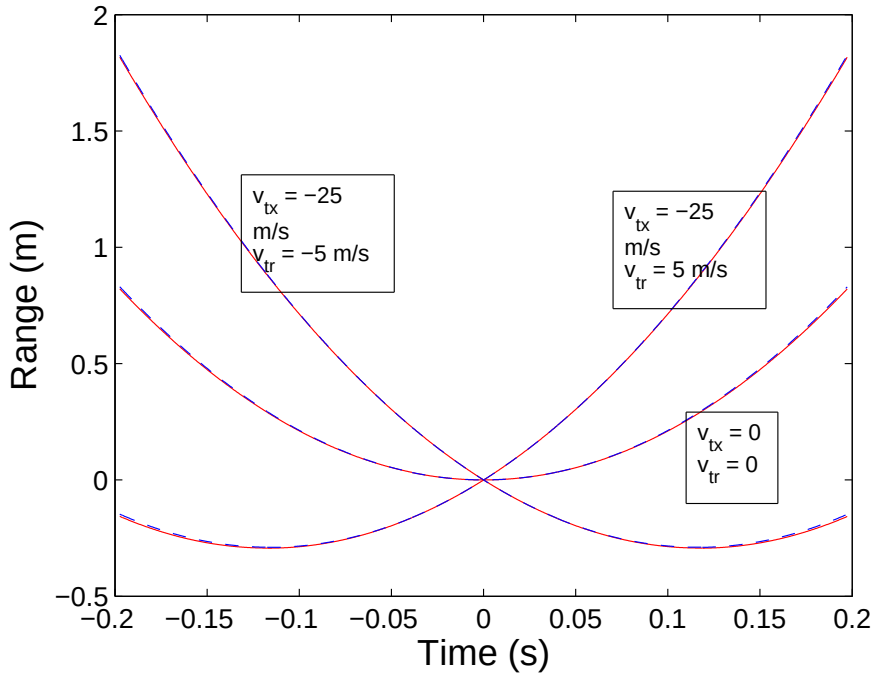

Figure 5: *Range histories of a target moving at three different velocities: (a)* $v_{tx} = 0$, $v_{tr} = 10$ *m/s, (b)* $v_{tx} = -25$, $v_{tr} = 5$ *m/s, and (c)* $v_{tx} = -25$ *m/s,* $v_{tr} = -5$ *m/s. The red lines are generated using the zero-motion Earth model and the blue lines are generated using the moving Earth model with a dynamic antenna squint compensation computed using (24). The 2-D model is used.*

not be accomplished using only one single antenna squint angle. The dependence of Earth motion compensation on the target azimuth velocity is an effect that needs to be taken into account in the development of a parameter estimation algorithm.

2.2 Simplified two-dimensional model

The range history of a moving target in a spherical geometry, Fig. 6(a), can be simplified as a target moving in a slant-range plane, Fig. 6(b), and is modelled as

$$\begin{aligned} R(t) =& \{[x_0 + v_x t - R_s \sin(\omega_s t)]^2 \\ &+ [r_0 + v_r t - R_s(1 - \cos(\omega_s t)) \cos\phi]^2\}^{\frac{1}{2}}, \end{aligned} \tag{25}$$

where ω_s is the satellite angular velocity, and $R_s = R_e + h_s$ is the spacecraft orbital radius. Subscript "0" denotes the target position at time zero; x and r are azimuth and slant-range directions, respectively, as defined in Fig. 6(b). As stated earlier, RADARSAT-2 performs yaw steering (i.e. a dynamic antenna beam squint) to compensate for the Earth rotation. As before, this antenna beam squint is modelled as

$$x_0 = r_0 \tan\phi_s + \delta x_0, \tag{26}$$

where δx_0 is the target azimuth position from the antenna beam center on the ground at time zero. The Earth rotation is modelled as

$$\begin{aligned} v_x &= v_{tx} + v_{ex}, \\ v_r &= v_{tr} + v_{er}, \end{aligned} \tag{27}$$

where v_{tx} and v_{tr} are target azimuth and slant-range velocities, respectively, and v_{ex} and v_{er} are the earth surface azimuth and slant-range velocities, respectively, at a particular latitude θ_{lat}. The target position, velocity, and acceleration (including the Earth motion) with respect to the radar can be shown to be

$$\boxed{\begin{aligned} \breve{x} &= x - x_s = x_0 + v_x t - R_s \sin(\omega_s t), \\ \breve{v}_x &= v_x - v_{sx} = v_x - R_s \cos(\omega_s t)\omega_s, \\ \breve{a}_x &= -a_{sx} = R_s \sin(\omega_s t)\omega_s^2, \\ \breve{r} &= r - r_s = r_0 + v_r t - R_s[1 - \cos(\omega_s t)] \cos\phi, \\ \breve{v}_r &= v_r - v_{sr} = v_r - R_s \sin(\omega_s t)\omega_s \cos\phi, \\ \breve{a}_r &= -a_{sr} = -R_s \cos(\omega_s t)\omega_s^2 \cos\phi, \end{aligned}} \tag{28}$$

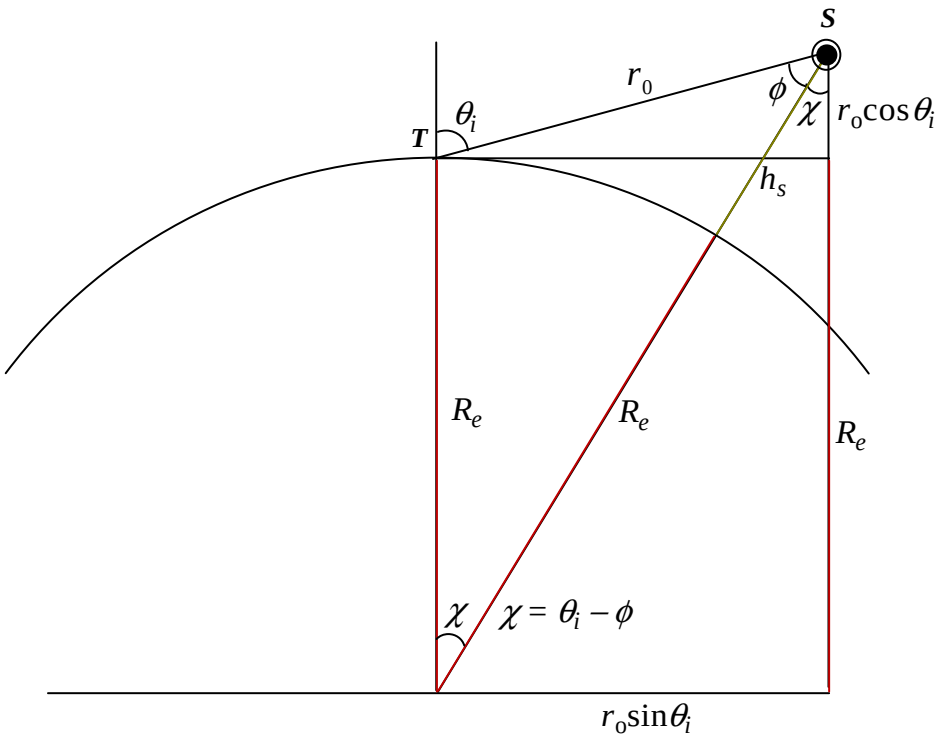

(a)

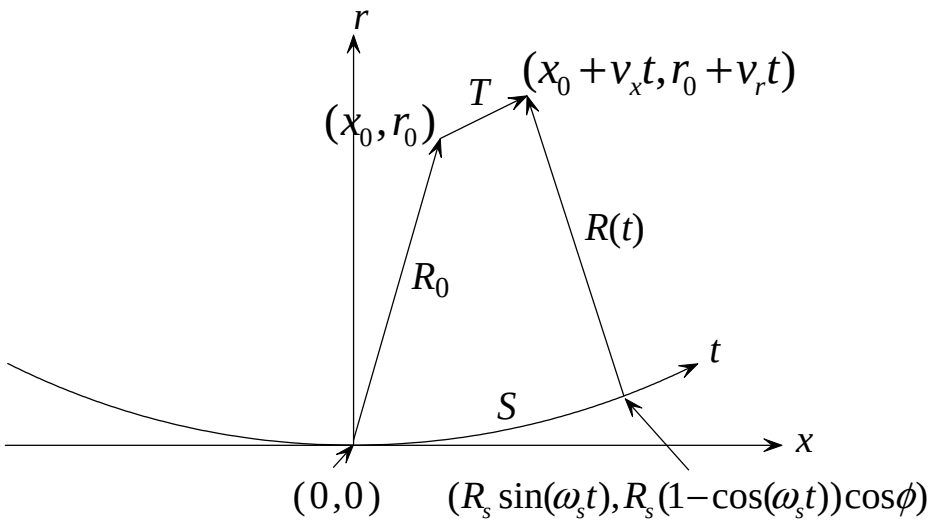

(b)

Figure 6: *(a) Spaceborne geometry showing radar flying out of the page; the spacecraft's orbital plane forms an angle ϕ with respect to the slant-range plane. (b) Slant-range geometry showing moving target and radar trajectories projected on the slant-range xr plane.*

where

$$\boxed{\begin{aligned} x &= x_0 + v_x t, \\ x_s &= R_s \sin(\omega_s t), \\ v_{sx} &= R_s \cos(\omega_s t)\omega_s, \\ a_{sx} &= -R_s \sin(\omega_s t)\omega_s^2, \\ r &= r_0 + v_r t, \\ r_s &= R_s[1 - \cos(\omega_s t)]\cos\phi, \\ v_{sr} &= R_s \sin(\omega_s t)\omega_s \cos\phi, \\ a_{sr} &= R_s \cos(\omega_s t)\omega_s^2 \cos\phi. \end{aligned}} \tag{29}$$

Defining time t_b to be when the target is in the middle of squinted beam, that is, $R_s \sin(\omega_s t_b) = \delta x_0 + v_x t_b$, then the Taylor expansion of (25) about t_b leads to

$$\boxed{R(t) \approx R_b + \dot{R}(t_b)(t - t_b) + \frac{\ddot{R}(t_b)}{2}(t - t_b)^2}, \tag{30}$$

where R_b, $\dot{R}(t_b)$, and $\ddot{R}(t_b)$ are derived below, and cubic and higher order terms have been neglected. The distance from radar to target at time t_b can be shown to be equal to

$$\begin{aligned} R_b &= \{[r_0 \tan\phi_s]^2 + [r_0 + v_{tr}t_b + v_{er}t_b - R_s(1 - \cos(\omega_s t_b))\cos\phi]^2\}^{1/2} \\ &\approx r_0(\tan^2\phi_s + 1)^{1/2}, \end{aligned} \tag{31}$$

where $v_{tr}t_b$, $v_{er}t_b$, and $R_s(1 - \cos(\omega_s t_b))\cos\phi$ are typically five to six orders of magnitude smaller than r_0 and are, therefore, neglected. Taking the derivative of (25) with respect t and substituting for $t = t_b$, one obtains

$$\begin{aligned} \dot{R}(t_b) &= \{[r_0 \tan\phi_s + \delta x_0 + v_x t_b - R_s \sin(\omega_s t_b)][v_x - R_s \cos(\omega_s t_b)\omega_s] \\ &\quad + [r_0 + v_r t_b - R_s(1 - \cos(\omega_s t_b))\cos\phi][v_r - R_s \sin(\omega_s t_b)\omega_s \cos\phi]\}/R_b \\ &= \{r_0 \tan\phi_s \breve{v}_x(t_b) + [r_0 + v_{tr}t_b + v_{er}t_b - r_s(t_b)]\breve{v}_r(t_b)\}/R_b \\ &\approx [r_0 \tan\phi_s \breve{v}_x(t_b) + r_0 \breve{v}_r(t_b)]/R_b. \end{aligned} \tag{32}$$

Again, $v_{tr}t_b$, $v_{er}t_b$, and $r_s(t_b)$ are neglected with respect to r_0. Equation (32) can be further simplified by taking note of the fact that the dynamic antenna squint is applied to "cancel" or compensate for the Earth's motion. Therefore, the squint angle ϕ_s should be chosen such that the terms containing $\tan\phi_s$ cancel out the terms containing the Earth motion (i.e. v_{ex} and v_{er}), that is

$$\begin{aligned} & r_0 \tan\phi_s \breve{v}_x(t_b) + r_0 \breve{v}_r(t_b) \\ &\qquad = r_0 \tan\phi_s[v_{tx} + v_{ex} - v_{sx}(t_b)] + r_0[v_{tr} + v_{er} - v_{sr}(t_b)] \\ &\qquad = r_0[v_{tr} - v_{sr}(t_b)]. \end{aligned} \tag{33}$$

This leads to the following equation:

$$\tan\phi_s[v_{tx} + v_{ex} - v_{sx}(t_b)] + v_{er} = 0, \tag{34}$$

which yields the formula (24) when solving for ϕ_s given that $v_{sx}(t_b) \approx v_s$. One notes that the dynamic antenna squint is originally intended for imaging stationary targets and therefore does not include the apparent "squint" introduced by a target moving in the along-track direction (i.e. $v_{tx} \neq 0$). Therefore, the parameter estimation algorithm to be developed in the next section does not include v_{tx} in the squint angle calculation; equation (21) is used instead. Therefore, when the Earth motion is compensated for using (21), equation (32) becomes

$$\dot{R}(t_b) = \frac{r_0(\tan\phi_s v_{tx} + v_{tr})}{R_b}, \tag{35}$$

where $v_{sr}(t_b)$, typically $<$ 0.1 m/s, has been ignored. The 2nd derivative of $R(t)$ can be similarly calculated and when it is evaluated at t_b gives

$$\ddot{R}(t_b) = [\breve{v}_x^2(t_b) + \breve{v}_r^2(t_b) - r_0\tan\phi_s a_{sx}(t_b) - r_0 a_{sr}(t_b)]/R_b, \tag{36}$$

where $(\bullet)^2/R_b^3$ and higher order terms have been neglected. The term $\breve{v}_r^2(t_b) = [v_r - R_s\sin(\omega_s t_b)\omega_s\cos\phi]^2 \approx v_r^2$, given that $v_{sr}(t_b)$ is over four orders of magnitude smaller than v_r, and $a_{sx}(t_b)$ can be neglected with respect to $a_{sr}(t_b)$ for the same reason. Therefore, equation (36) can be approximated as

$$\ddot{R}(t_b) \approx \{[v_x - v_{sx}(t_b)]^2 + v_r^2 - r_0 a_{sr}(t_b)\}/R_b. \tag{37}$$

3 Parameter Estimation Based on Fractional Fourier Transform

We describe here a target parameter estimation algorithm based on the fractional Fourier transform (FrFT, see Appendix A) and along-track interferometry [15] for the spaceborne geometry. The FrFT is first applied to each detected target to maximize the displaced phase center antenna (DPCA) output signal by mapping the signal onto a fractional Fourier axis. The target's along-track interferometric phase ψ, measured at the maximum DPCA output, can be shown to be related to both across-track and along-track velocities of the target. This is due to RADARSAT-2's antenna squint, which introduces the along-track velocity dependence of ψ in the direction of radar-to-target line of sight. The result differs from that of the non-squint case, which depends mainly only on the target's across-track velocity component [14] when there is a negligible offset δt (to be discussed below) in the range history of the target with respect to time t_b. The derivation of target's interferometric phase

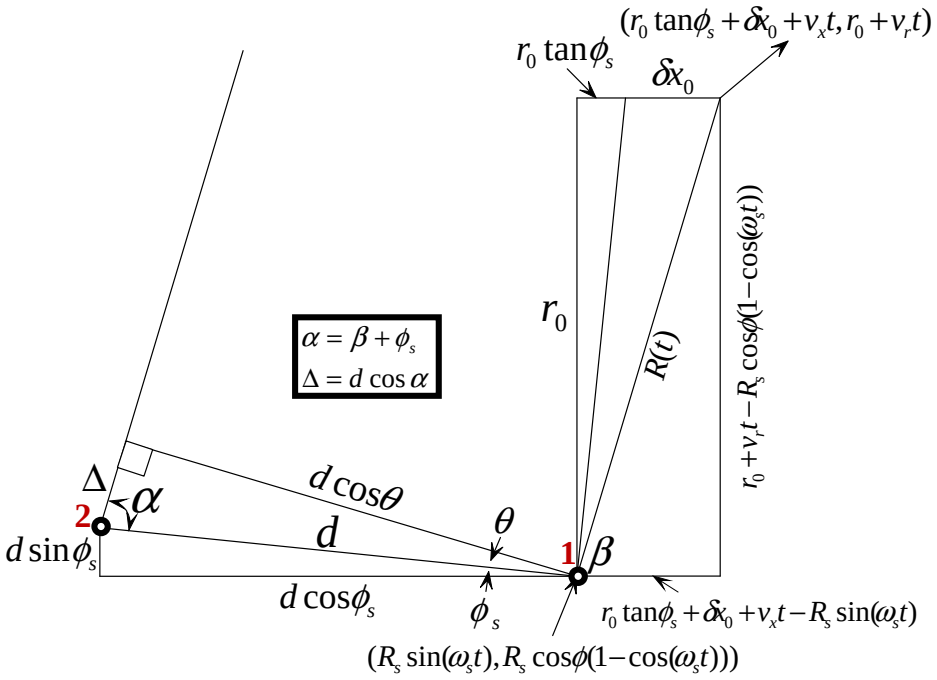

Figure 7: *Far-field approximation showing path difference Δ of the fore and aft apertures and the squint angle ϕ_s, and d is the distance between the two physical aperture centers.*

for the spaceborne geometry, with an antenna squint angle ϕ_s, is given below and is very similar to the case of an airborne platform with no antenna squinting [14]. The phase measured at the fore aperture can be written, using Taylor approximation (30), as

$$\varphi_1(t) = -2k\left[R_b + \gamma\hat{v}_r(t-t_b) + \frac{v_{rel}^2}{2R_b}(t-t_b)^2\right], \tag{38}$$

where

$$\boxed{\begin{array}{l}\gamma = r_0/R_b, \\ \hat{v}_r = \tan\phi_s v_{tx} + v_{tr}, \\ v_{rel}^2 = [v_x - v_{sx}(t_b)]^2 + v_r^2 - r_0 a_{sr}(t_b), \\ k = 2\pi/\lambda. \end{array}} \tag{39}$$

In the far-field approximation, the range history of the target for the aft aperture can be written as $R_2(t) = R_1(t) + \Delta$, where Δ is the one-way path difference between the two phase centers. Figure 7 illustrates the far-field geometry with an antenna squint angle ϕ_s. From the figure, it can be seen that

$$\begin{aligned}\Delta &= d\cos\alpha = d\cos(\beta+\phi_s) \\ &= d(\cos\beta\cos\phi_s - \sin\beta\sin\phi_s) \\ &= d(u\cos\phi_s - v\sin\phi_s),\end{aligned} \tag{40}$$

where $u = \cos\beta$ and $v = \sin\beta$, and d is the distance between the two phase centers. Again, using the geometry in Figure 7, u and v can be shown to be

$$\begin{aligned}u(t) = \cos(\beta) &= \frac{r_0\tan\phi_s + \delta x_0 + v_x t - R_s\sin(\omega_s t)}{R(t)}, \\ v(t) = \sin(\beta) &= \frac{r_0 + v_r t - R_s\cos\phi[1-\cos(\omega_s t)]}{R(t)}.\end{aligned} \tag{41}$$

The Taylor expansion of $u(t)$ and $v(t)$ about t_b and retaining only the first order terms (higher order terms are negligible), yields

$$\begin{aligned}u(t) &\approx \frac{v_x - v_{sx}(t_b)}{R_b}(t-t_b), \\ v(t) &\approx \frac{v_r - v_{sr}(t_b)}{R_b}(t-t_b),\end{aligned} \tag{42}$$

where $(\bullet)/R_b^2$ terms have been ignored. The second term in the last line of (40), $v\sin\phi_s$, can be shown to be about three orders of magnitude smaller ($< 1.4\times10^{-3}$) than the first term, $u\cos\phi_s$, and is neglected in the following derivation. The phase measured at the aft aperture can, therefore, be written as

$$\begin{aligned}\varphi_2(t) &= -2kR_1(t) - 2kd\frac{v_x - v_{sx}(t_b)}{R_b}\cos\phi_s(t-t_b) \\ &= \varphi_1(t) - kD\frac{v_x - v_s}{R_b}(t-t_b),\end{aligned} \tag{43}$$

where $D = 2d\cos\phi_s$ and $v_{sx}(t_b) \approx v_s$ (the satellite velocity). Co-registering the aft channel with the fore channel gives

$$\begin{aligned}
\varphi_2\left(t+\frac{D}{2v_s}\right) =& -2kR_b - 2k\gamma\hat{v}_r\left(t-t_b+\frac{D}{2v_s}\right) - \frac{kv_{rel}^2}{R_b}\left(t-t_b+\frac{D}{2v_s}\right)^2 \\
& - \frac{kD(v_x-v_s)}{R_b}\left(t-t_b+\frac{D}{2v_s}\right) \\
=& -2kR_b - 2k\gamma\hat{v}_r(t-t_b) - \frac{k\gamma\hat{v}_r D}{v_s} \\
& - \frac{kv_{rel}^2}{R_b}(t-t_b)^2 - \frac{kv_{rel}^2 D}{R_b v_s}(t-t_b) - \cancelto{0}{\frac{kv_{rel}^2 D^2}{4v_s^2 R_b}} \\
& - \frac{k(v_x-v_s)D}{R_b}(t-t_b) - \cancelto{0}{\frac{k(v_x-v_s)D^2}{2v_s R_b}} \\
=& \varphi_1(t) - \frac{k\gamma\hat{v}_r D}{v_s} - \frac{kv_{rel}^2 D}{R_b v_s}(t-t_b) - \frac{k(v_x-v_s)D}{R_b}(t-t_b),
\end{aligned} \tag{44}$$

where the strike-through terms are considered negligible. If the actual measured target range history (i.e. when the target is actually visible to radar) is centered at $t = t_b + \delta t$, where δt is an offset in the range history of the target, then the co-registered signals at apertures 1 and 2 can be written, respectively, as

$$\begin{aligned}
s_1 &= \text{rect}\left[\frac{t-t_b-\delta t}{T}\right] e^{j\varphi_1(t)}, \\
s_2 &= \text{rect}\left[\frac{t-t_b-\delta t}{T}\right] e^{j\varphi_2(t+D/2v_s)},
\end{aligned} \tag{45}$$

where T ($\gg D/2v_s$) is the length of the signal. Substituting (45) into (A.1) and integrating to maximize the target signal in the fractional Fourier domain yields obtains

$$\begin{aligned}
F_{\alpha 1}(u) &= e^{j\epsilon_1}\int_{-\infty}^{+\infty} \text{rect}\left[\frac{t-t_b-\delta t}{T}\right] e^{j(\xi_1 t+\nu_1 t^2)}dt \\
&= e^{j\epsilon_1}\int_{t_b+\delta t-T/2}^{t_b+\delta t+T/2} e^{j\xi_1 t}dt = e^{j\epsilon_1}\frac{e^{j\xi_1 t}}{j\xi_1}\Bigg|_{t_b+\delta t-T/2}^{t_b+\delta t+T/2} \\
&= e^{j[\epsilon_1+\xi_1(t_b+\delta t)]}\frac{2}{\xi_1}\frac{e^{j\xi_1 T/2}-e^{-j\xi_1 T/2}}{2j} \\
&= e^{j[\epsilon_1+\xi_1(t_b+\delta t)]}T\frac{\sin(\pi\xi_1 T/2\pi)}{\pi\xi_1 T/2\pi} \\
&= e^{j[\epsilon_1+\xi_1(t_b+\delta t)]}T\,\text{sinc}\left(\frac{\xi_1 T}{2\pi}\right),
\end{aligned} \tag{46}$$

where

$$\epsilon_1 = -2kR_b + 2k\gamma\hat{v}_r t_b - \frac{kv_{rel}^2 t_b^2}{R_b} + 2\pi a u^2, \tag{47}$$

$$\xi_1 = -2k\gamma\hat{v}_r + \frac{2kv_{rel}^2 t_b}{R_b} - 4\pi abu, \tag{48}$$

and

$$\nu_1 = -\frac{kv_{rel}^2}{R_b} + 2\pi a = 0. \tag{49}$$

Note that u is the fractional frequency variable and should not be confused with u in (41) and (42). The target signal amplitude is maximized in the fractional Fourier domain if ν_1 is set equal to zero, which yields a "sinc" function in (46) and the optimum fractional angle α ($a = \cot\alpha/2$):

$$\alpha = \text{acot}\left(\frac{kv_{rel}^2}{\pi R_b}\right). \tag{50}$$

Because the discrete FrFT deals with frequency and time samples rather than Hertz and seconds, one must convert them to frequency and time samples, which yields v_{rel}^2 as

$$\boxed{v_{rel}^2 = \frac{\pi R_b f_s^2}{kN}\cot\alpha}, \tag{51}$$

where f_s is the pulse repetition frequency and N is the total number of azimuth samples.

Similarly, the optimum fractional Fourier transform of the signal received at channel 2 can be shown to be

$$F_{\alpha 2}(u) = e^{j[\epsilon_2 + \xi_2(t_b+\delta t)]} T\,\text{sinc}\left(\frac{\xi_2 T}{2\pi}\right), \tag{52}$$

where

$$\epsilon_2 = \epsilon_1 - \frac{k\gamma\hat{v}_r D}{v_s} + \frac{kDt_b}{R_b}v_e, \tag{53}$$

$$\xi_2 = \xi_1 - \frac{kD}{R_b}v_e, \tag{54}$$

$$\boxed{v_e = \frac{v_{rel}^2}{v_s} + v_x - v_s}. \tag{55}$$

Therefore, the phase of interferogram ($\arg[F_{\alpha 1}(u)F_{\alpha 2}(u)^*]$) or the ATI phase ($\psi$) evaluated at the optimum fractional Fourier angle α yields

$$\begin{aligned}\psi &= \epsilon_1 + \xi_1(t_b+\delta t) - [\epsilon_2 + \xi_2(t_b+\delta t)] \\ &= \epsilon_1 - \epsilon_2 + (\xi_1 - \xi_2)(t_b+\delta t) \\ &= \frac{kD\hat{v}_r\gamma}{v_s} - \frac{kDv_e}{R_b}t_b + \frac{kDv_e}{R_b}(t_b+\delta t) \\ &= \frac{kD\hat{v}_r\gamma}{v_s} + \frac{kDv_e}{R_b}\delta t,\end{aligned} \tag{56}$$

which indicates that ψ is sensitive to v_x contained in both $\hat{v}_r$ and v_e. If the target range history is centered at t_b, then v_e dependence vanishes.

The positions of a moving target in the fractional Fourier axis for channels 1 and 2 can be derived by setting $\xi_1 = 0$ and $\xi_2 = 0$. Evaluating at the maxima of the "sinc" functions in (46) and (52) yields

$$u_1 = \frac{1}{4\pi ab}\left(-2k\gamma\hat{v}_r + \frac{2kv_{rel}^2 t_b}{R_b}\right), \tag{57}$$

$$u_2 = \frac{1}{4\pi ab}\left(-2k\gamma\hat{v}_r + \frac{2kv_{rel}^2 t_b}{R_b} - \frac{kv_{rel}^2 D}{R_b v_s} - \frac{k(v_x - v_s)D}{R_b}\right). \tag{58}$$

The third and fourth terms in (58) can be ignored compared to the first term ($\sim 10^3\times$ smaller than the first term and $\sim 50\times$ smaller than the second term), and $\|u_1 - u_2\|$ is smaller than the spatial resolution of "sinc" functions, implying spatial overlap on the fractional Fourier axis. Therefore one can set $u_1 = u_2 = u_p$ and the target azimuth position x_b ($= r_0 \tan\phi_s + v_s t_b$) can be obtained directly from (57) by solving for t_b:

$$t_b = \frac{R_b}{v_{rel}^2}\left(\frac{\pi u_p}{k\sin\alpha} + \gamma v_y\right). \tag{59}$$

Converting Hertz-second to frequency-time samples, (59) becomes

$$\boxed{t_b = \left(\frac{f_s^2}{N}\right)\frac{R_b}{v_{rel}^2}\left(\frac{\pi u_p}{k\sin\alpha} + \gamma\hat{v}_r\right)}. \tag{60}$$

For unregistered channels, the ATI phase can be similarly derived. The phase of a signal at channel 2 is

$$\varphi_2(t) = \varphi_1(t) - \frac{k(v_x - v_s)D}{R_b}(t - t_b), \tag{61}$$

and the fractional Fourier transform of the signal at channel 2 is

$$\begin{aligned}F_{\alpha 2}(u) &= e^{j\epsilon_{2u}}\int_{-\infty}^{+\infty}\text{rect}\left[\frac{t - t_b - \delta t}{T}\right]e^{j(\xi_{2u}t + \nu_{2u}t^2)}dt \\ &= e^{j[\epsilon_{2u} + \xi_{2u}(t_b+\delta t)]}T\,\text{sinc}\left(\frac{\xi_{2u}T}{2\pi}\right),\end{aligned} \tag{62}$$

where

$$\epsilon_{2u} = \epsilon_1 + \frac{k(v_x - v_s)t_b D}{R_b}, \tag{63}$$

$$\xi_{2u} = \xi_1 - \frac{k(v_x - v_s)D}{R_b}, \tag{64}$$

and $\nu_{2u} = 0$. Therefore the unregistered ATI phase is

$$\begin{aligned}
\psi_u &= \epsilon_1 + \xi_1(t_b + \delta t) - [\epsilon_{2u} + \xi_{2u}(t_b + \delta t)] \\
&= \epsilon_1 - \epsilon_{2u} + (\xi_1 - \xi_{2u})(t_b + \delta t) \\
&= -\frac{k(v_x - v_s)t_b D}{R_b} + \frac{k(v_x - v_s)D}{R_b}(t_b + \delta t) \\
&= \frac{k(v_x - v_s)D}{R_b}\delta t.
\end{aligned} \tag{65}$$

Equation (65) is used to eliminate the additional unknown parameter δt due to the offset in the broadside time t_b. Substituting

$$\delta t = \frac{R_b \psi_u}{k(v_x - v_s)D} \tag{66}$$

into (56), one obtains

$$\psi = \frac{k\gamma \hat{v}_r D}{v_s} + \frac{v_e}{v_x - v_s}\psi_u, \tag{67}$$

and solving for v_{tr} yields

$$v_{tr} = \frac{v_s}{k\gamma D}\left\{\psi - \psi_u\left[\frac{v_{rel}^2}{v_s(v_{tx} + v_{ex} - v_s)} + 1\right]\right\} - \tan\phi_s v_{tx}. \tag{68}$$

Parameters α, ψ, and ψ_u are measured experimentally. Therefore, v_{tx} and v_{tr} can be solved using (51) and (68). Then t_b is obtained by substituting v_{tx} and v_{tr} into (60). From equations (27), (29), and (39), we get

$$v_{tx} = \sqrt{v_{rel}^2 + r_0 R_s \omega_s^2 \cos\phi - (v_{tr} + v_{er})^2} + v_s - v_{ex} \tag{69}$$

In summary, the equations used in estimating v_{tx}, v_{tr}, and t_b ($x_b = r_0 \tan\phi_s + v_s t_b$) are

$$\boxed{\begin{aligned}
v_{tx} &= \sqrt{v_{rel}^2 + r_0 R_s \omega_s^2 \cos\phi - (v_{tr} + v_{er})^2} + v_s - v_{ex}, \\
v_{tr} &= \frac{v_s}{k\gamma D}\left\{\psi - \psi_u\left[\frac{v_{rel}^2}{v_s(v_{tx} + v_{ex} - v_s)} + 1\right]\right\} - \tan\phi_s v_{tx}, \\
t_b &= \frac{f_s^2 R_b}{N v_{rel}^2}\left[\frac{\pi u_p}{k\sin\alpha} + \gamma(\tan\phi_s v_{tx} + v_{tr})\right].
\end{aligned}} \tag{70}$$

4 Conclusions

The fractional Fourier transform (FrFT) is used both to maximize the signal-to-clutter ratio and to allow target parameters to be estimated in the fractional Fourier domain using a few derived equations. The target parameter algorithm based on the fractional Fourier transform has been developed previously for airborne (flat stationary Earth) geometry and tested using Convair 580 data. Subtle differences exist in migrating from a flat stationary Earth geometry to a spherical rotating Earth geometry. Factors, such as orbital parameters and spacecraft centripetal acceleration, must be taken into account. In addition, the dynamic antenna squint implemented in RADARSAT-2 satellite for Earth motion compensation needs to be modelled into the algorithm. A signal model describing a target moving on a spherical rotating Earth is developed. This signal model is rigorous but its usefulness is limited, in that it cannot be expressed easily in a non-vector form that can be readily used to construct the target's range history and the SAR reference function. A simplified two-dimensional signal model is developed and the spherical three-dimensional model is used to verify equivalence. Using the simplified model, the target parameter estimation algorithm is derived for RADARSAT-2's MODEX and tested using simulated data. This work is the first to address moving target parameter estimation in the RADARSAT-2 MODEX context. Although the developed parameter estimation algorithm is applied to two-aperture SAR data, the technique can be extended to three- or four-aperture systems.

References

1. Livingstone, C.E. 1998. The addition of MTI modes to commercial SAR satellites. *Proc. of 10th CASI Conference on Astronautics*, Ottawa, Canada, 26-28 October 1998, pp. 267-275.

2. Gierull, C.H. and Sikaneta, I.C. 2003. Raw data based two-aperture SAR ground moving target indication. In IGARSS'2003, *Proceedings of the International Geoscience and Remote Sensing Symposium*, Toulouse, France, 21-25 July.

3. Stockburger, E.F. and Held, D.N. 1995. Interferometric moving ground target imaging. *The Record of the IEEE 1995 International Radar Conference*, pp. 438-443.

4. Yadin, E. 1996. A performance evaluation model for a two port interferometer SAR-MTI. *Proceedings of the 1996 IEEE National Radar Conference*, pp. 261-266.

5. Ender, J.H.G. 1999. Space-time processing for multichannel synthetic aperture radar. Electronics & Communication Engineering Journal, Vol. 11 (1), pp. 29-38.

6. Livingstone, C.E. and Thompson, A.A. 2004. The moving object detection experiment on RADARSAT-2. Can. J. Remote Sensing, Vol. 30, No. 3, pp. 355-368.

7. Coe, D.J. and White, R.G. 1995. Moving target detection in SAR imagery: experimental results. *The Record of the IEEE 1995 Internatinal Radar Conference*, pp. 644-649.

8. Raney, R.K. 1971. Synthetic aperture imaging radar and moving targets. IEEE Transactions on Aerospace and Electronic Systems, Vol. 7, No. 3, pp. 499-505.

9. Gierull, C. H. and Livingstone, C. 2004. SAR-GMTI concept for RADARSAT-2, in *The Applications of Space-Time Processing*, R. Klemm, Ed. IEE Press, Stevenage, UK.

10. Sikaneta, I. C. and Chouinard, J.-Y. 2004. Eigendecomposition of the multi-channel covariance matrix with applications to SAR-GMTI, Signal Processing, vol. 84, No. 9 (Special Issue), pp. 1501–1535.

11. Gierull, C. H. 2004. Statistical analysis of multilook SAR interferograms for CFAR detection of ground moving targets, IEEE Trans. Geosci. Remote Sensing, Vol. 42, No. 4, pp. 691–701, April.

12. Gierull, C. H. 2002. Moving target detection with along-track SAR interferometry - a theoretical analysis (DRDC TR 2002-084) Defence R&D Canada - Ottawa.

13. Livingstone, C.E., Sikaneta, I., Gierull, C.H., Chiu, S., Beaudoin, A., Campbell, J., Beaudoin, J., Gong, S., Knight, T.A. 2002. An airborne SAR experiment to support RADARSAT-2 GMTI. Can. J. Remote Sensing, Vol. 28, No. 6, pp. 794-813.

14. Chiu, S. 2004. Two-channel SAR-GMTI via fractional Fourier transform (DRDC TM 2004-172) Defence R&D Canada - Ottawa.

15. Chiu, S. 2005. Application of fractional Fourier Transform to moving target indication via along-track interferometry. In special issue “Advances in Interferometric Synthetic Aperture Radar Processing,” EURASIP Journal on Applied Signal Processing 20, pp. 3293-3303.

16. Almeida, L.B. 1994. The fractional Fourier transform and time-frequency representations. IEEE Trans. Signal Processing, Vol. 42, No. 11, pp. 3084-3091.

17. Zayed, A.I. 1996. On the relationship between the Fourier and fractional Fourier transforms. IEEE Trans. Signal Processing Letters, Vol. 3, No. 12, pp. 310-311.

18. Dickey, F.R., Jr., Santa, M.M. 1953. Final report on anticlutter techniques, General Electric Company Report. R65EMH37, 1 March.

19. Chiu, S. 2003. Clutter effects on ground moving target velocity estimation with SAR along-track interferometry. In IGARSS’2003, *Proceedings of the International Geoscience and Remote Sensing Symposium*, Toulouse, France, 21-25 July.

20. Sharma, J.J. and Collins, M.J. 2004. Focusing accelerating ground moving targets in SAR imagery. In EUSAR’2005, *Proceedings of 5th European Conference on Synthetic Aperture Radar*, Ulm, Germany, 25-27 May.

Annex A
Fractional Fourier transform

The fractional Fourier transform (FrFT) with rotational angle α of a signal $f(t)$ is defined as [16], [17]

$$F_\alpha(u) = \Re^\alpha[f](u) = \int_{-\infty}^{\infty} f(t) K_\alpha(t,u) dt, \tag{A.1}$$

where, for α not equal to zero or a multiple of π, the kernel $K_\alpha(t,u)$ is given by

$$K_\alpha(t,u) = c e^{j2\pi a[t^2+u^2-2but]}, \tag{A.2}$$

and

$$a = \frac{\cot\alpha}{2}, \quad b = \sec\alpha, \quad c = \sqrt{1 - j\cot\alpha}. \tag{A.3}$$

The FrFT with parameter α can be considered as a generalization of the conventional Fourier transform (FT). Thus, the FrFT for $\alpha = \pi/2$ and $\alpha = -\pi/2$ reduces to the conventional and inverse FT, respectively. Multiplying both sides of (A.1) by $e^{-j2\pi a u^2}$, one obtains

$$e^{-j2\pi a u^2} F_\alpha(u) = \widetilde{F}_\alpha(u) = c \int_{-\infty}^{\infty} f(t) e^{j2\pi a(t^2-2but)} dt. \tag{A.4}$$

Substituting $\nu/2ab$ for u in (A.4), it becomes

$$\begin{aligned} \widetilde{F}_\alpha\left(\frac{\nu}{2ab}\right) &= c \int_{-\infty}^{\infty} f(t) e^{j2\pi(at^2-\nu t)} dt \\ &= \int_{-\infty}^{\infty} \left[c f(t) e^{j2\pi a t^2}\right] e^{-j2\pi\nu t} dt \\ &= \int_{-\infty}^{\infty} g_\alpha(t) e^{-j2\pi\nu t} dt \\ &= G_\alpha(\nu). \end{aligned} \tag{A.5}$$

The second last line in (A.5) shows that the FrFT is a variation of the standard FT. As such, many of its properties, such as its inverse formula and sampling theorems for band-limited and time-limited signals, can be easily derived from those of the FT by a simple change of variable. With respect to the parameter α, the FrFT is continuous, periodic ($\Re^\alpha = \Re^{\alpha+2\pi n}$, with n an integer) and additive ($\Re^\alpha \Re^\beta = \Re^{\alpha+\beta}$), and has the symmetry relation $\Re^\alpha[f^*](u) = \{\Re^{-\alpha}[f](u)\}^*$. The inverse FrFT can thus be written as

$$f(t) = \Re^{-\alpha}[F_\alpha](t) = \int_{-\infty}^{\infty} F_\alpha(u) K_{-\alpha}(t,u) du. \tag{A.6}$$

The FrFT maps the signal onto a rotated (or fractional) frequency axis such that the originally slanted chirp energy becomes perpendicular to the rotated axis and, thus, highly compressed or focused as illustrated in Figure A.1. Also shown in Figure A.1 (insert) is a "measured" moving target mapped onto the optimum fractional frequency axis. The target energy, as can be seen, is highly compressed. Note that the clutter has been suppressed via the Displaced Phase Center Antenna (DPCA) technique [18]. The residual clutter (plus noise) surrounding the signal chirp can be further filtered out if desired. The signal strength is dramatically increased due to pulse compression, resulting in a significant improvement in the signal-to-clutter ratio (SCR) and, thus, in the interferometric phase estimation accuracy [12], [19].

The pulse compression via the FrFT is more or less equivalent to SAR azimuth processing via a matched filter that matches to the coefficient of the second order term (i.e. the slope of the chirp) in (30) or (37). The signal compression via the FrFT is not dependent on the first order term (i.e. the Doppler shift) but only on second and higher order terms in the Taylor expansion, in contrast to the matched filter approach, and will lead to a fully focused target if the target is moving at a constant velocity throughout the synthetic aperture time or only slightly accelerating in the across-track direction. Unlike a matched filter, which is capable of fully "matching" to the target's motion if the motion parameters are known, the FrFT cannot, in principle, fully focus a target that is accelerating in the along-track direction (i.e. $a_x \neq 0$) because a_x introduces nonlinearity into the signal chirp. The across-track acceleration, on the other hand, introduces mainly a Doppler-rate change in the chirp and, therefore, does not lead to significant nonlinearity [20].

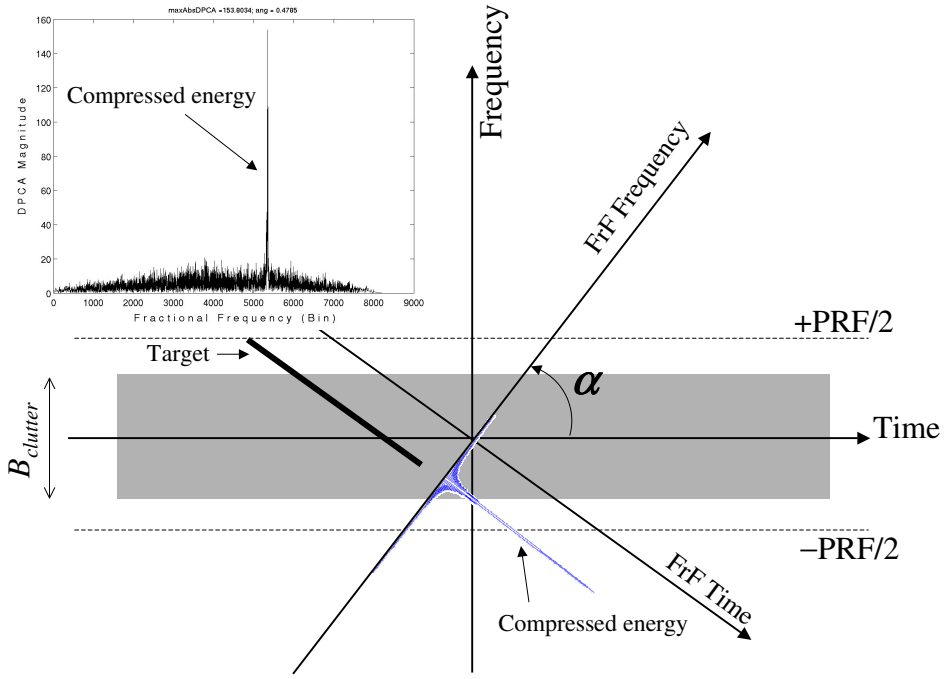

Figure A.1: *Illustrating a target energy focused via the FrFT. The insert shows an actual moving target's signal compressed in the fractional frequency domain.*

Annex B
MATLAB Code ‘calOrbPar.m’

The following Matlab code computes the range history of a moving target in spherical orbital geometry using propagation vectors and transformation matrices.

```
clear all

%This is a spherical geometry orbital approach to model RADARSAT-2
%MODEX. It is been shown that the 2-D approach ('spaceSigGen.m')
%produces the exactly same signal as this full-orbital approach
%('calOrbPar.m').

%physical constants
G = 6.67e-11; %gravitational constant
Me = 5.98e24; %mass of the Earth
re = 6372.795477598e3; %quadratic mean radius of the Earth
hs = 800e3; %spacecraft altitude
rs = re + hs; %spacecraft orbital radius
c = 3e8; %speed of light

%geometry parameters
theta_i = 50*pi/180; %angle of incidence
phi = asin((re/(re+hs))*sin(theta_i)); %angle of depression
psi = theta_i-phi; %angle:  beam center's radial & spacecraft's radial
inclination = 98.6*pi/180;
tilt = inclination-pi/2;
rotZ = 50*pi/180; %angle measured from Equinox
ws = sqrt((G*Me)/rs^3); %spacecraft angular velocity
vs = ws*rs; %spacecraft velocity
we = 2*pi/(23*60^2+56*60+4.09); %earth angular velocity
thetaPos0 = 40*pi/180; %angle from equator along orbit track at t=0
r0 = rs*sin(psi)/sin(theta_i); %slant range at time=0

%radar parameters
fc = 5.405e9; %radar center frequency
lambda = c/fc;
fs = 3800; %pulse repetition frequency
tpri = 1/fs;
d = 7.5/2; %distance between phase centers (corrected)
tdpca = d/vs;
```

```
shift_incr = tdpca/tpri;

%generate time vector t and antenna gain pattern b
%N = 1501; %for short run used only
N = 2*13750+1;
delta_t = 0;
Theta = 0.4; %in degree
theta = Theta*pi/180; %degree beamwidth to radian beamwidth
x = r0*tan(theta/2);
beamWidth = 2*x/vs;
T = beamWidth-2*abs(delta_t);

%transformation matrices
Mx = [1 0 0; 0 cos(tilt) -sin(tilt); 0 sin(tilt) cos(tilt)];
My0 = [cos(thetaPos0) 0 -sin(thetaPos0); 0 1 0; sin(thetaPos0) 0 cos(thetaPos0)];
Mz = [cos(rotZ) -sin(rotZ) 0; sin(rotZ) cos(rotZ) 0; 0 0 1];
L = [0 re*sin(psi) 0]';

%earth angular velocity vector
We = we*[0 0 1]';

%satellite orbital angular velocity vector
Ws = ws*[0 -1 0]';
Ws = Mz*Mx*Ws;

%generate state vectors at time = 0
Rp0 = Mz*Mx*((My0*re*cos(psi)*[1 0 0]')+L);
Ve0 = cross(We,Rp0);
Rs0 = Mz*Mx*My0*rs*[1 0 0]';
Vp0 = cross(Ws,Rp0); %beam ground velocity at point 'P'
Vs0 = cross(Ws,Rs0);

%compute unit vectors
uni_x = Vp0/absVec(Vp0); %along track
uni_y = cross(Vp0,Rp0)/absVec(cross(Vp0,Rp0)); %across track
uni_sr = (Rp0-Rs0)/absVec(Rp0-Rs0); %across track in slant range

%components of earth velocity in ground range and azimuth
vex0 = dot(Ve0,uni_x);
ver0 = dot(Ve0,uni_sr);
vey0 = dot(Ve0,uni_y);
```

```
%target parameters
vtx = 0; %target azimuth velocity
vtr = 0;
vty = vtr/sin(theta_i); %target range velocity
delta_x0 = 0;
vsx0 = vs;
phi_s = atan(ver0/(vsx0-vex0));
x0 = r0*tan(phi_s) + delta_x0; %target initial azimuth position

%compute the latitude and longitude at Rp0
arg_WeRp0 = acos(dot(We,Rp0)/(absVec(We)*absVec(Rp0)))*180/pi;
theta_lat = 90-arg_WeRp0 %latitude of beam center on ground at t=0
Rp0xy = Rp0;
Rp0xy(3) = 0;
theta_long = acos(dot(Rp0xy,[1 0 0]')/absVec(Rp0xy))*180/pi %longitude

%signal generation loop
for n = 1:N
t = ((n-1)-(N-1)/2)*tpri;
n %display loop number

%time-dependent y-rotation matrix
My = [cos(thetaPos0+ws*t) 0 -sin(thetaPos0+ws*t); 0 1 0; sin(thetaPos0+ws*t)
0 cos(thetaPos0+ws*t)];

%compute satellite orbital motion vector Rs
Rs = rs*[1 0 0]';
Rs = Mz*Mx*My*Rs;

%compute satellite nadir point vector on the ground (not used)
Rn = re*[1 0 0]';
Rn = Mz*Mx*My*Rn;

%compute equator vector (not used)
Req = re*[1 0 0]';
Mze = [cos(ws*t) -sin(ws*t) 0; sin(ws*t) cos(ws*t) 0; 0 0 1];
Req = Mze*Req;

%compute radar beam track vector on the ground
Rp = re*cos(psi)*[1 0 0]';
Rp = Mz*Mx*((My*Rp)+L);
```

```
%compute target motion vector
%There is a very slight difference between 'r' and 'y' approaches
Rt = Rp0 + (x0+(vtx+vex0)*t)*uni_x + (vtr+ver0)*t*uni_sr;
%Rt = Rp0 + (x0+(vtx+vex0)*t)*uni_x + (vty+vey0)*t*uni_y; %'y' approach
Rt0 = Rp0 + x0*uni_x;
R0 = absVec(Rt0-Rs0);

%construct range history array
R_Array(n,:,:,:)  = absVec(Rt-Rs) - R0;
t_Array(n) = t;
end %for loop

%plot range history figure; plot(t_Array,R_Array);
```

Annex C
MATLAB Code ‘spaceSigGen.m’

The following Matlab code computes the range histories of a moving target using a simplified 2-D slant range geometry model for fore and aft channels. It then generates a reference function to azimuth-compress the signals before forming an along-track interferogram.

```
clear all

%This is a 2-D approach to RADARSAT-2 MODEX.
%It has been shown that this 2-D approach ('spaceSigGen.m') produces
%exactly the same signal as the spherical orbital approach ('calOrbPar.m').

%constants
G = 6.67e-11; %gravitational constant
Me = 5.98e24; %mass of the Earth
Re = 6372.795477598e3; %quadratic mean radius of the Earth
hs = 800e3; %spacecraft altitude
Rs = Re+hs;
c = 3e8; %speed of light

%geometry parameters
theta_i = 50*pi/180; %angle of incidence
theta_L = 40.4801*pi/180; %latitude
phi = asin((Re/Rs)*sin(theta_i)); %angle of depression
psi = theta_i-phi; %look angle
ws = sqrt((G*Me)/Rs^3); %spacecraft angle velocity
vs = Rs*ws; %spacecraft velocity
we = 2*pi/(23*60^2+56*60+4.06);
r0 = Rs*sin(psi)/sin(theta_i) %slant range at time zero

%radar parameters
fc = 5.405e9; %radar center frequency
lambda = c/fc;
fs = 3800; %pulse repetition frequency
tpri = 1/fs;
d = 7.5/2; %distance between phase centers (corrected)
tdpca = d/vs;
shift_incr = tdpca/tpri;
```

```
%target parameters
vtx = 25;
vtr = -5;
vex = -32.3766; %calculated from orbital parameters
ver = 269.5196; %calculated from orbital parameters
vx = vtx + vex ;
vr = vtr + ver;
delta_x0 = 100;
tb = delta_x0/(Rs*ws-vx);
vsxb = Rs*cos(ws*tb)*ws;
phi_s = atan(ver/(vsxb-vex));
x0 = r0*tan(phi_s) + delta_x0;

%choice parameters (not yet used)
simClut = 1;
%inv_scr = 10;
plotHist = 1;

%initial range
R0 = sqrt(r0^2 + (r0*tan(phi_s) + delta_x0)^2)

%generate time vector t and antenna gain pattern b
delta_t = 0;
Theta = 0.35; %in degree
theta = Theta*pi/180; %degree beamwidth to radian beamwidth
x = r0*tan(theta/2);
beamWidth = 2*x/vs;
%N = 1501; %for short run use only
N = 2*13750;
t = -(N-1)/2:(N-1)/2; t = t*tpri;
T = beamWidth-2*abs(delta_t);
%b1 = rectpuls(t-tb-delta_t,T); % true pulse center is half of shift
in rectpuls
b1 = (sinc(1.2*(t-tb+delta_t)/(beamWidth))).^2;
b2 = (sinc(1.2*(t-tdpca-tb+delta_t)/(beamWidth))).^2;

%generate reference signal
tc = 0; %should be set to zero always
t0 = tc+T/2:-tpri:tc-T/2; %time reversed t0 = -t
Ref1 = sqrt((x0 + vx*t0 - Rs*sin(ws*t0)).Ĝ + (r0 + vr*t0 - Rs*(1 -
cos(ws*t0))*cos(phi)).^2) - R0;
Ref2 = sqrt((x0 + vx*t0 - Rs*sin(ws*(t0-tdpca))).^2 + (r0 + d*sin(phi_s)
```

```
+ vr*t0 - Rs*(1 - cos(ws*(t0-tdpca)))*cos(phi)).^2) - R0;
%Ref2 = sqrt((x0 + vx*t0 - Rs*sin(ws*(t0-tdpca))).^2 + (r0 + vr*t0
- Rs*(1 - cos(ws*(t0-tdpca)))*cos(phi)).^2) - R0;
ref1 = exp(-j*4*pi*Ref1/lambda);
ref2 = exp(-j*4*pi*Ref2/lambda);
%figure; plot(t0,real(ref))

%generate pulses in slow time
R1 = sqrt((x0 + vx*t - Rs*sin(ws*t)).^2 + (r0 + vr*t - Rs*(1 - cos(ws*t))*
cos(phi)).^2) - R0;
figure; plot(t,R1)
s1o = b1.*exp(-j*4*pi*R1/lambda);
%figure; plot(t,real(s1o))
% tfPlotSig(s1o,fs)

R2 = sqrt((x0 + vx*t - Rs*sin(ws*(t-tdpca))).^2 + (r0 + d*sin(phi_s)
+ vr*t - Rs*(1 - cos(ws*(t-tdpca)))*cos(phi)).^2) - R0;
%R2 = sqrt((x0 + vx*t - Rs*sin(ws*(t-tdpca))).^2 + (r0 + vr*t - Rs*(1
- cos(ws*(t-tdpca)))*cos(phi)).^2) - R0;
%figure; plot(t,R2)
s2u = b2.*exp(-j*4*pi*R2/lambda);
s2o = (shiftM(s2u',shift_incr))'; %coregistration
%figure; plot(t,real(s2o))

%Frequency-domain azimuth compression - Method #2:
%using Radix-2 FFT
Naz = length(s1o) + length(ref1) - 1;
p_length1 = 2^(ceil(log10(Naz)/log10(2) - 2*1e-7));

S1 = fft(s1o,p_length1);
REF1 = fft(conj(ref1),p_length1);
Z1 = S1.*REF1;
z1 = ifft(Z1);
z1 = z1(1:Naz);
%figure; plot(abs(z1));

S2 = fft(s2o,p_length1);
REF2 = fft(conj(ref2),p_length1);
Z2 = S2.*REF2;
z2 = ifft(Z2);
z2 = z2(1:Naz);
%figure; plot(abs(z2));
```

```
%compute interferogram
ati = z1.*conj(z2);
% figure; plot(abs(z1));
figure; polar(angle(ati),abs(ati),'.');

clear all
```

Annex D
MATLAB Code ‘spaceFormulas.m’

The following program generates simulated RADARSAT-2 MODEX signals, applies fractional Fourier transform (FrFT) on the signals, and computes interferograms from the FrFT compressed signals. The phase of the interferogram is compared with the theoretical value computed from equation (56). The results show that the theoretical results agree with those obtained from the simulation.

```
clear all

%constants
G = 6.67e-11; %gravitational constant
Me = 5.98e24; %mass of the Earth
Re = 6372.795477598e3; %quadratic mean radius of the Earth
hs = 800e3; %spacecraft altitude
Rs = Re + hs; %spacecraft orbital radius
c = 3e8; %speed of light

%geometry parameters
incTheta = 50*pi/180; %angle of incidence
phi = asin((Re/(Re + hs))*sin(incTheta)); %angle of depression
psi = incTheta - phi; %look angle
ws = sqrt((G*Me)/Rs^3); %spacecraft angle velocity
r0 = Rs*sin(psi)/sin(incTheta); %slant range at time zero

%target parameters with earth motions
vtx = -20;
vtr = 25;
vex = -32.3766; %calculated from orbital parameters
ver = 269.5196; %calculated from orbital parameters
vx = vtx + vex;
vr = vtr + ver;
%this number should NOT be too large!!!  Or else ver and vex should
%be modified to correspond to new lat & long
delta_x0 = -100;
tb = delta_x0/(Rs*ws-vx) %this is a good approximation
ws*tb %check the approximation above
sin(ws*tb) %check approximation above

%spacecraft parameters
```

```
vsxb = Rs*cos(ws*tb)*ws;
asxb = -Rs*sin(ws*tb)*ws^2;
phi_s = atan(ver/(vsxb-vex));

%relative parameters
x0 = r0*tan(phi_s) + delta_x0;
R0 = sqrt(x0^2 + r0^2) %initial range (at t = 0)

%radar parameters
fc = 5.405e9; %radar center frequency
lambda = c/fc;
k = 2*pi/lambda; %wavenumber
fs = 3800; %pulse repetition frequency
tpri = 1/fs;
d = 7.5/2; %distance between phase centers
D = d*cos(phi_s); %true DPCA distance in along-track direction
tdpca = D/vsxb;
shift_incr = tdpca/tpri;

%generate time vector t and antenna gain pattern b
delta_t = 0.2;
Theta = 0.38; %azimuth beamwidth in degree
theta = Theta*pi/180; %convert degree beamwidth to radian beamwidth
x = r0*tan(theta/2);
beamWidth = 2*x/vsxb; %beamwidth expressed in time unit
N = 2*13750; %total number of samples
t = -(N-1)/2:(N-1)/2; t = t*tpri;
T = beamWidth-2*abs(delta_t);
b = rectpuls(t-tb-delta_t,T); % true new pulse center is half of shift
in rectpuls
%b = (sinc((t-tb-delta_t)/T)).^2;

%calculate intermediate parameters
%Rb = sqrt((r0*tan(phi_s) + delta_x0 + vx*tb - Rs*sin(ws*tb))^2 + (r0
+ vr*tb - Rs*(1 - cos(ws*tb))*cos(phi))^2)
Rb = sqrt((r0*tan(phi_s))^2 + (r0 + vr*tb - Rs*(1 - cos(ws*tb))*cos(phi))^2);
vsrb = Rs*sin(ws*tb)*ws*cos(phi);
asrb = Rs*cos(ws*tb)*ws^2*cos(phi);
vrel = sqrt((vx - vsxb)^2 + vr^2 - r0*asrb); %note the complete expression
yields exactly the same result
%vrel = sqrt((vx - vsxb)^2 + (vr - vsrb)^2 - r0*tan(phi_s)*asxb - r0*asrb)
ve = vrel^2/vsxb + (vx - vsxb)
```

```
vr_hat = tan(phi_s)*vtx + vtr;
gamma = r0/Rb;

%calculate theoretical alpha
alpha = acot(k*vrel^2*N/(pi*Rb*fs^2));

%generate pulses in slow time
%Channel 1
R1 = sqrt((x0 + vx*t - Rs*sin(ws*t)).^2 + (r0 + vr*t - Rs*cos(phi)*
(1-cos(ws*t))).^2);
%R1 = Rb + gamma*vr_hat*(t-tb) + vrel^2*(t-tb).^2/(2*Rb);
figure; plot(t,R1)
%s1 = b.*exp(-j*4*pi*R1/lambda);
s1 = b.*exp(-j*2*k*R1);
figure; plot(t, real(s1))

a = alpha/(pi/2);
z1 = fracF(s1,a);
figure; plot(abs(z1)); title(['a = ', num2str(a)]);

%Channel 2
%The discrepacies between the far field approximation and "exact"
%equation is that in exact approach, the aft aperture is delayed in
%BOTH azimuth and range directions.  The question:  is this model
%correct?  NO! The aft aperture should not be delayed in range direction!

% R2 = sqrt((x0 + vx*t - (Rs - d*sin(phi_s))*sin(ws*(t-tdpca))).^2
+ (r0 + vr*t ...
% - (Rs*cos(phi)*(1 - cos(ws*t)) + d*sin(phi_s)*cos(ws*t))).^2);

%These are alternate R2 expression which give approximately the same
result
% R2 = sqrt((x0 + vx*t - Rs*sin(ws*(t-tdpca))).^2 + (r0 + vr*t ...
% - ((Rs + d*sin(phi_s))*(1 - cos(ws*t))*cos(phi))).^2);
% R2 = sqrt((x0 + vx*t - Rs*sin(ws*(t-tdpca))).^2 + (r0 + vr*t ...
% - (Rs*cos(phi)*(1 - cos(ws*t)) + d*sin(phi_s))).^2);

%The far-field approximation give the same result as the exact equations
xrelb = r0*tan(phi_s);% + delta_x0 + vx*t - Rs*sin(ws*t);
rrelb = r0 + vr*tb - Rs*cos(phi)*(1-cos(ws*tb));
% v5 = 2*xrelb*(vx-vsxb) + 2*rrelb*(vr-vsrb);
% deltab = D*xrelb/Rb - rrelb*d*sin(phi_s)/Rb;
```

```
% delta_dotb = D*((vx-vsxb)/Rb );%- xrelb^2*(vx-vsxb)/Rb^3 + ...
%xrelb*rrelb*(vr-vsrb)/Rb^3) - d*sin(phi_s)*(vr-vsrb)/Rb + ...
%rrelb*sin(phi_s)*(xrelb*(vx-vsxb) + rrelb*(vr-vsrb))/Rb^3;
% delta_2dotsb = d*(-asxb*cos(phi_s)/Rb - (vx-vsxb)*cos(phi_s)*v5/Rb^3
+ ...
%(3/4)*xrelb*cos(phi_s)*v5^2/Rb^5 - xrelb*cos(phi_s)*((vx-vsxb)^2 +
...
%xrelb*(-asxb) + (vr-vsrb)^2 - rrelb*asrb)/Rb^3 + asrb*sin(phi_s)/Rb
+ ...
%(vr-vsrb)*sin(phi_s)*v5/Rb^3 - (3/4)*rrelb*sin(phi_s)*v5^2/Rb^5 +
...
%rrelb*sin(phi_s)*((vx-vsxb)^2 + xrelb*(-asxb) + (vr-vsrb)^2 - ...
%rrelb*asrb)/Rb^3);
% delta = delta_dotb*(t-tb);% + deltab ;%+ delta_2dotsb*(t-tb).^2/2;
% R2 = R1 + delta;

R2 = R1 + D*(vx - vsxb)*(t-tb)/Rb;
%R2 = R1 + (D*(vx - vsxb) - d*sin(phi_s)*(vr - vsrb))*(t-tb)/Rb;
%s2u = b.*exp(-j*4*pi*R2/lambda);
s2u = b.*exp(-j*2*k*R2);
s2 = (shiftM(s2u',-shift_incr))'; %coregistration
z2 = fracF(s2,a);

% %channel 3
% R3 = sqrt((x0 + vx*t - Rs*sin(ws*(t-2*tdpca))).^2 + (r0 + vr*t ...
% - (Rs*(1 - cos(ws*(t-2*tdpca)))*cos(phi) + 2*d*sin(phi_s))).^2) -
R0;
% s3u = b.*exp(-j*4*pi*R3/lambda);
% s3 = (shiftM(s3u',-2*shift_incr))'; %coregistration
% z3 = fracF(s3,a);

%calculate theoretical ATI phases
%extra = k*(D*xrelb/Rb - d*sin(phi_s)*rrelb/Rb)
phi_ATI = (k*gamma*vr_hat*2*D/vsxb + k*2*D*ve*delta_t/Rb)*180/pi

%compute interferogram
%channels 12
ati12 = z1.*conj(z2);
figure; polar(angle(ati12),abs(ati12),'.');
[Imag12,J] = max(abs(ati12));
atiPhase_max12 = angle(ati12(J,1))*180/pi %ATI phase measured at maximum
ATI magnitude
```

```
err_ATI_phase = abs(phi_ATI - atiPhase_max12);
title(['Measured ATI Phase 1&2 = ', num2str(atiPhase_max12)]);
xlabel(['Calculated Theoretical ATI Phase = ', num2str(phi_ATI)]);
ylabel(['ATI Phase Error = ', num2str(err_ATI_phase)]);

%channels 23
ati23 = z2.*conj(z3);
figure; polar(angle(ati23),abs(ati23),'.');
[ATImag23,J] = max(abs(ati23));
atiPhase_max23 = angle(ati23(J,1))*180/pi %ATI phase measured at maximum
ATI magnitude
title(['Measured ATI Phase 2&3 = ', num2str(atiPhase_max23)]);
xlabel(['Calculated Theoretical ATI Phase = ', num2str(phi_ATI)]);

%dpca12
dpca12 = z1 - z2;
dpca23 = z2 - z3;
ati = dpca12.*conj(dpca23);
figure; polar(angle(ati),abs(ati),'.');
[ATImag,J] = max(abs(ati));
atiPhase_max = angle(ati(J,1))*180/pi %ATI phase measured at maximum
ATI magnitude
title(['Measured ATI Phase 1&2DPCA = ', num2str(atiPhase_max)]);
xlabel(['Calculated Theoretical ATI Phase = ', num2str(phi_ATI)]);
```

DOCUMENT CONTROL DATA

(Security classification of title, body of abstract and indexing annotation must be entered when document is classified)

1. ORIGINATOR (the name and address of the organization preparing the document. Organizations for whom the document was prepared, e.g. Centre sponsoring a contractor's report, or tasking agency, are entered in section 8.)

Defence R&D Canada - Ottawa
3701 Carling Avenue, Ottawa, Ontario K1A 0Z4, Canada

2. SECURITY CLASSIFICATION (overall security classification of the document including special warning terms if applicable).

UNCLASSIFIED

3. TITLE (the complete document title as indicated on the title page. Its classification should be indicated by the appropriate abbreviation (S,C,R or U) in parentheses after the title).

Moving Target Parameter Estimation for RADARSAT-2 MODEX

4. AUTHORS (Last name, first name, middle initial. If military, show rank, e.g. Doe, Maj. John E.)

Chiu, S.

5. DATE OF PUBLICATION (month and year of publication of document)

December 2005

6a. NO. OF PAGES (total containing information. Include Annexes, Appendices, etc).

49

6b. NO. OF REFS (total cited in document)

20

7. DESCRIPTIVE NOTES (the category of the document, e.g. technical report, technical note or memorandum. If appropriate, enter the type of report, e.g. interim, progress, summary, annual or final. Give the inclusive dates when a specific reporting period is covered).

Technical Memorandum

8. SPONSORING ACTIVITY (the name of the department project office or laboratory sponsoring the research and development. Include address).

Defence R&D Canada - Ottawa
3701 Carling Avenue, Ottawa, Ontario K1A 0Z4, Canada

9a. PROJECT OR GRANT NO. (if appropriate, the applicable research and development project or grant number under which the document was written. Specify whether project or grant).

15eg

9b. CONTRACT NO. (if appropriate, the applicable number under which the document was written).

N/A

10a. ORIGINATOR'S DOCUMENT NUMBER (the official document number by which the document is identified by the originating activity. This number must be unique.)

DRDC Ottawa TM 2005-214

10b. OTHER DOCUMENT NOs. (Any other numbers which may be assigned this document either by the originator or by the sponsor.)

11. DOCUMENT AVAILABILITY (any limitations on further dissemination of the document, other than those imposed by security classification)

(X) Unlimited distribution
( ) Defence departments and defence contractors; further distribution only as approved
( ) Defence departments and Canadian defence contractors; further distribution only as approved
( ) Government departments and agencies; further distribution only as approved
( ) Defence departments; further distribution only as approved
( ) Other (please specify):

12. DOCUMENT ANNOUNCEMENT (any limitation to the bibliographic announcement of this document. This will normally correspond to the Document Availability (11). However, where further distribution beyond the audience specified in (11) is possible, a wider announcement audience may be selected).

Unlimited

13. ABSTRACT (a brief and factual summary of the document. It may also appear elsewhere in the body of the document itself. It is highly desirable that the abstract of classified documents be unclassified. Each paragraph of the abstract shall begin with an indication of the security classification of the information in the paragraph (unless the document itself is unclassified) represented as (S), (C), (R), or (U). It is not necessary to include here abstracts in both official languages unless the text is bilingual).

Moving target parameter estimation algorithms have been developed previously for airborne (or flat Earth) geometry. Subtle differences exist in migrating from a flat stationary Earth geometry to a spherical rotating Earth geometry. Factors, such as orbital parameters and spacecraft centripetal acceleration, must be taken into account. In addition, the dynamic antenna squint implemented in the RADARSAT-2 satellite for Earth motion compensation needs to be modelled into the algorithms. This technical memorandum derives the spaceborne version of the algorithm, based on the fractional Fourier transform and along-track interferometry, previously developed for the Convair 580 radar.

14. KEYWORDS, DESCRIPTORS or IDENTIFIERS (technically meaningful terms or short phrases that characterize a document and could be helpful in cataloguing the document. They should be selected so that no security classification is required. Identifiers, such as equipment model designation, trade name, military project code name, geographic location may also be included. If possible keywords should be selected from a published thesaurus. e.g. Thesaurus of Engineering and Scientific Terms (TEST) and that thesaurus-identified. If it not possible to select indexing terms which are Unclassified, the classification of each should be indicated as with the title).

Synthetic Aperture Radar (SAR), Fractional Fourier Transform, Ground Moving Target Indication (GMTI), Spaceborne Radar, Parameter Estimation

Defence R&D Canada

Canada's leader in Defence
and National Security
Science and Technology

R & D pour la défense Canada

Chef de file au Canada en matière
de science et de technologie pour
la défense et la sécurité nationale

www.drdc-rddc.gc.ca